Geochemistry Geophysics Geosystems G3

Article
Volume 13, Number 10
16 October 2012
Q10011, doi:10.1029/2012GC004201
ISSN: 1525-2027

Published by AGU and the Geochemical Society

The character of seafloor ambient noise recorded offshore New Zealand: Results from the MOANA ocean bottom seismic experiment

Zhaohui Yang and Anne F. Sheehan

Department of Geological Sciences, University of Colorado Boulder, Boulder, Colorado 80309, USA (zhaohuiyang@gmail.com)

Cooperative Institute for Research in Environmental Sciences, University of Colorado Boulder, Boulder, Colorado 80309, USA

John A. Collins

Department of Geology and Geophysics, Woods Hole Oceanographic Institution, Woods Hole, Massachusetts 02543, USA

Gabi Laske

Institute of Geophysics and Planetary Physics, University of California, San Diego, La Jolla, California 92093-0225, USA

[1] We analyze the characteristics of ambient noise recorded on ocean-bottom seismographs using data from the 2009–2010 MOANA (Marine Observations of Anisotropy Near Aotearoa) seismic experiment deployed west and east of South Island, New Zealand. Microseism and infragravity noise peaks are clear on data recorded on the vertical channel of the seismometer and on the pressure sensor. The noise levels in the infragravity band (<0.03 Hz) on the horizontal seismometer channels are too high to show the infragravity peak. There is a small difference (~0.25 Hz versus ~0.2 Hz) in microseism peak frequencies between the two sides of the South Island on all three seismic channels. Our results show clear depth dependence between the peak frequency of infragravity waves and the water depth. We find that the product of water depth and wave number at the peak frequency is a constant, $k_oH = 1.5$. This relationship can be used to determine the variation of phase and group velocity of infragravity waves with water depth, and the location of the infragravity peak and corresponding noise notch at any water depth. These estimates of spectral characteristics, particularly low noise bands, are useful for future OBS deployments.

Components: 4600 words, 5 figures.

Keywords: New Zealand; OBS; continental shelf; infragravity wave; noise.

Index Terms: 4560 Oceanography: Physical: Surface waves and tides (1222); 7294 Seismology: Seismic instruments and networks (0935, 3025).

Received 23 April 2012; **Revised** 10 September 2012; **Accepted** 11 September 2012; **Published** 16 October 2012.

Yang, Z., A. F. Sheehan, J. A. Collins, and G. Laske (2012), The character of seafloor ambient noise recorded offshore New Zealand: Results from the MOANA ocean bottom seismic experiment, *Geochem. Geophys. Geosyst.*, *13*, Q10011, doi:10.1029/2012GC004201.

©2012. American Geophysical Union. All Rights Reserved.

1. Introduction

[2] Studying seafloor ambient noise is important for both improving the performance of ocean-bottom seismographs (OBS) [e.g., *Webb*, 1998; *Collins et al.*, 2001], and understanding the generation and propagation processes of oceanic noise sources [e.g., *Webb et al.*, 1991; *Bromirski et al.*, 2005; *Dolenc et al.*, 2005, 2008]. *Webb* [1998] presents a comprehensive review of seafloor noise in the seismic band. In general, seismic noise can be separated into three different bands: higher than 1 Hz, 1–0.05 Hz, and lower than 0.05 Hz. Microseismic noise dominates between 1 and 0.05 Hz, which is the result of nonlinear-wave interaction of wind-generated ocean gravity waves, including the "double frequency peak" [*Longuet-Higgins*, 1950] and "single frequency peak" [*Hasselmann*, 1963]. Below 0.05 Hz, noise levels increase abruptly and the noise from infragravity waves dominates [e.g., *Webb et al.*, 1991].

[3] The Marine Observations of Anisotropy Near Aotearoa (MOANA) is an ocean-bottom seismic experiment carried out offshore the South Island of New Zealand that was designed to explore the rheology and deformation in the lithosphere. The OBS stations were deployed from the deep ocean to the continental slope at depths between 550 m and 4700 m (Figure 1 and Table S1 in the auxiliary material), providing a good opportunity to study the variation of seafloor ambient noise with depth.[1] In this study, we conduct a noise analysis for the MOANA data set in order to quantify and characterize the ambient noise levels at each site, with a particular emphasis on the infragravity wave band.

2. Data and Method

[4] As part of the MOANA experiment, 30 OBS were deployed for one year (January 2009 to February 2010) west and east of the South Island, New Zealand. The OBS are part of the U.S. Ocean Bottom Seismic Instrument Pool (OBSIP), and the instruments used were provided by the Scripps Institution of Oceanography (SIO) Institutional Instrument Center (IIC). In addition to the OBS sites, four broadband seismometers were deployed on the South Island of New Zealand (Figure 1) as land references for the OBS.

[5] Of the 30 OBS, 29 were equipped with a Nanometrics Trillium 240 broadband seismometer, and one was equipped with a Nanometrics Trillium 40 intermediate-period seismometer. All 30 OBS carried a Differential Pressure Gauge (DPG) [*Cox et al.*, 1984]. All stations were planned to record continuously for a year with a sampling rate of 50 sps before being recovered in early 2010. The seismometer on station NZ01 malfunctioned throughout the deployment but the DPG functioned normally. Station NZ15 was trawled up by a New Zealand fishing vessel in June/July 2009 (J. A. Collins et al., unpublished MOANA Recovery Cruise Report, 2010) and fortunately both instrument and data were recovered. Station NZ17 washed ashore at an unknown date and was recovered in 2011. Data from the rest of the OBS stations were recovered from January 2009 to February 2010.

[6] We carry out our noise analysis using the software package PQLX [*McNamara and Buland*, 2004; *McNamara and Boaz*, 2006]. This package uses probability density functions (PDF) to display the distribution of seismic power spectral density (PSD) [*McNamara and Buland*, 2004]. This approach has several advantages over the traditional PSD analysis. First, it does not require the screening of the continuous waveform for days without transient signals. These transient signals (earthquakes, data gaps, clipping, mass re-centering, calibration pulses, etc.) are generally low-probability events, and are thus easily distinguished from ambient seismic noise [*McNamara and Buland*, 2004], and do not affect the high-probability characteristic ambient seismic noise observed in PDFs. Second, PDFs for a specific station present a range of PSDs, which gives an overview of noise level fluctuations, providing much more information than a single PSD.

[7] PSDs for each seismic channel (BHZ, BH1, and BH2) at each station are computed from continuous, overlapping (50%) one-hour long time series segments. For each time segment, instrument responses are removed from data to generate ground acceleration for direct comparison to the new low noise model (NLNM) and the new high noise model (NHNM) of *Peterson* [1993]. Each one-hour long time series segment is divided into 13 sub-segments, overlapping by 75% in order to reduce the variance of final PSD estimation [*McNamara and Buland*, 2004], which leads to a stable spectra up to 100 s. For every sub-segment the mean and the long-period trend is removed, the time series is tapered with a 10% sine function, Fourier transformed to obtain the amplitude spectrum, and the amplitude is squared to obtain the power spectral density (PSD). The

[1] Auxiliary materials are available in the HTML. doi:10.1029/2012GC004201.

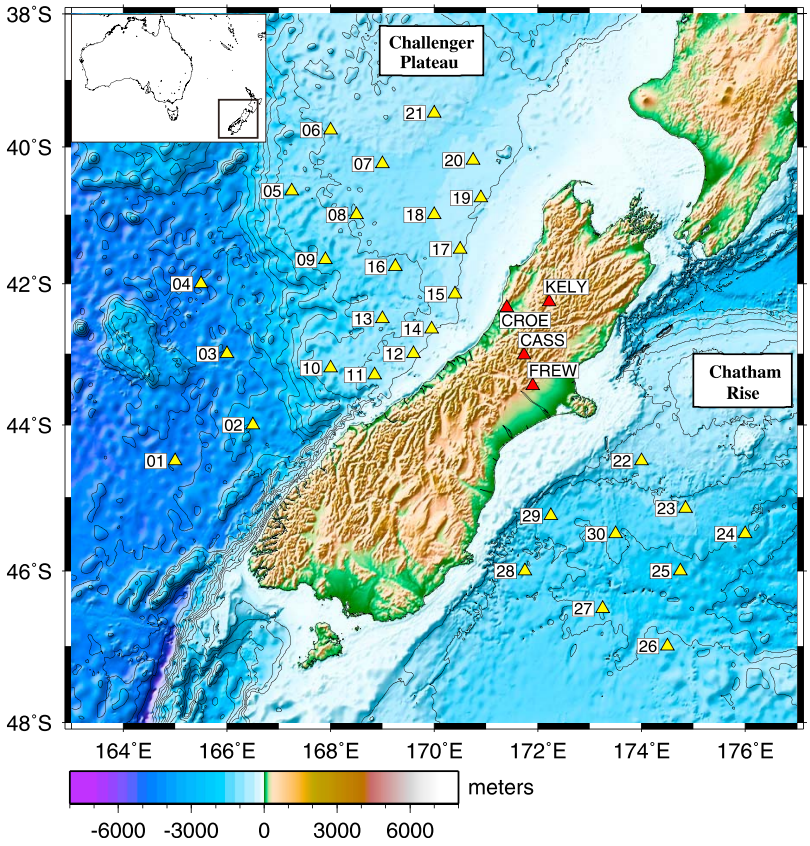

Figure 1. Map showing topography and bathymetry of New Zealand and offshore area. Yellow triangles represent Ocean-Bottom Seismographs (OBS) deployed during the seismic experiment MOANA. Red triangles are land stations deployed in the same seismic experiment. The deployment duration was from 2009/01 to 2010/02.

PSDs are gathered by binning periods in 1/8 octave intervals and binning power in one-dB intervals. To construct an empirical PDF, each period-power bin is normalized by the total number of contributing segments. For the DPG channel (BDH), we calculate the PSDs using Matlab codes, and for the seismic channels we use the PQLX software.

2.1. Comparison With Land Stations

[8] At land stations, noise between periods of 0.1 and 1.0 s mainly comes from wind turbulence and human activities [e.g., *Withers et al.*, 1996; *Wilson et al.*, 2002]. As OBS stations are underwater and often far away from coasts, OBS stations are usually quieter than land stations over this frequency band [e.g., *McCreery*, 1992; *Bradley et al.*, 1997]. Particularly, the vertical channels of deep ocean stations (4000 m and deeper) in our experiment are quieter by up to 30 dB than those of land stations in the short period band (<0.2 s) (Figures 2 and 3a; see also Figure S1 in the auxiliary material). Horizontal components are relatively noisier than vertical components. The ground response to local fluctuations of atmospheric pressure contributes significantly to long-period (>20 s) background noise of land stations [*Sorrells*, 1971]. Oceanic infragravity waves are the dominant noise source for vertical-component OBS data at periods longer than 30 s (Figures 2 and 3). Tilting of the seismometer brought about by seafloor currents results in very high noise levels on the horizontal components. [*Webb*, 1988; *Collins et al.*, 2001; *Duennebier and Sutton*, 2007, and references therein] (Figure 3).

[9] Between 1 s and 20 s, the PSDs are dominated by microseismic noise (Figures 2 and 3). The broad noise peak at 4–8 s with high magnitude is called the "double-frequency peak," and is caused by nonlinear interaction between the oceanic waves of equal period traveling in opposite directions [*Longuet-Higgins*, 1950]. The amplitude of the double-frequency peak on the ocean floor is higher than that seen on land stations by about 10–20 dB [$10\log(m^2/s^4/Hz)$] (Figure 3). The amplitudes of the double-frequency peak seem to be related to station depths, e.g., the deep sea stations, which are further from the ocean surface, have smaller amplitudes

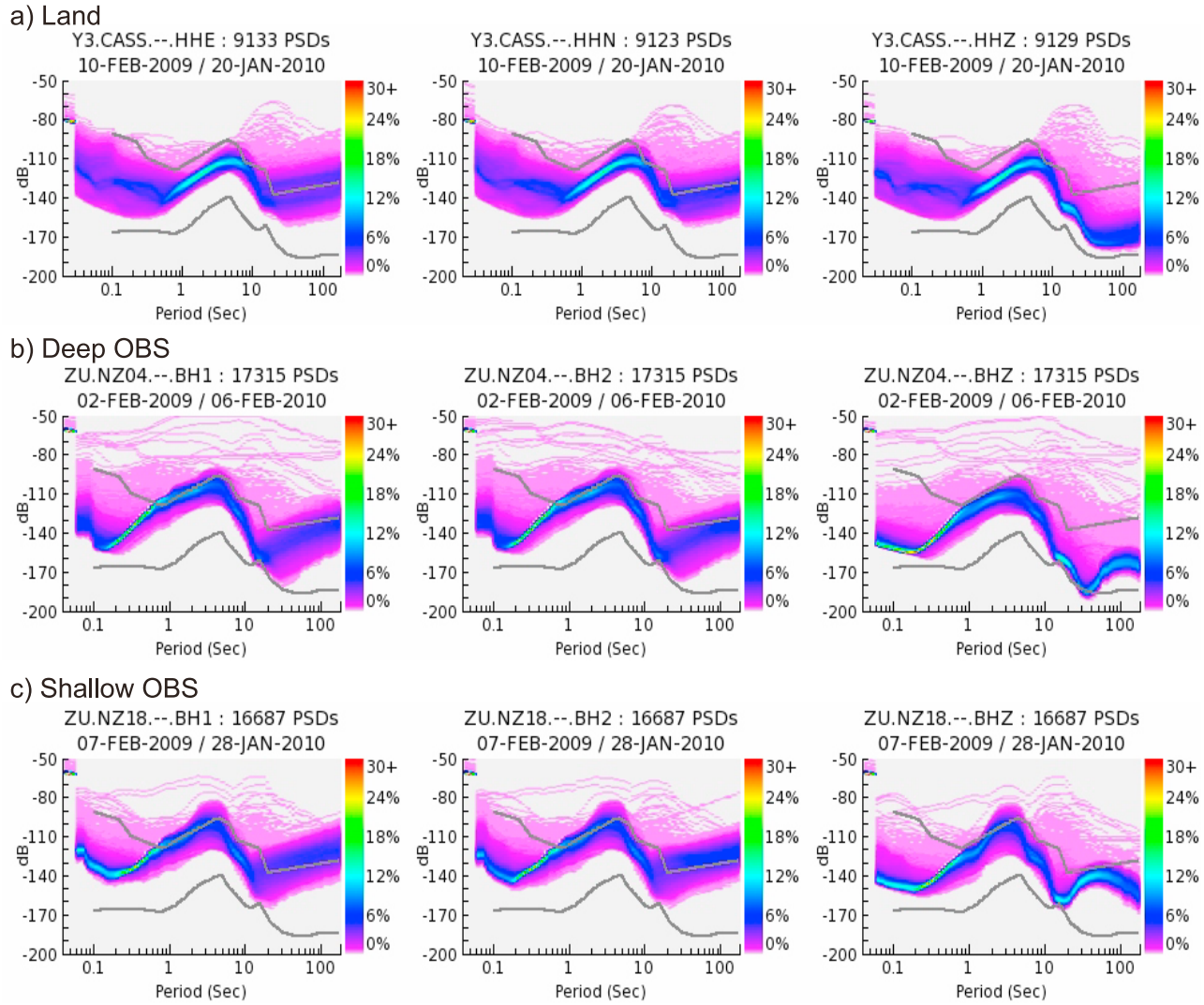

Figure 2. Power Density Functions (PDFs) of PSDs of three stations deployed during MOANA seismic experiment. The units on the *y* axis are $10\log(m^2/s^4/Hz)$, referred as dB. PDFs of other OBS stations are displayed in Figure S1 in Text S1 in the auxiliary material. (a) PDFs of an OBS station NZ18, which is 805 m below sea level. Horizontal 1 (BH1), Horizontal 2 (BH2), and Vertical channels (BHZ) are shown from left to right. (b) PDFs of an OBS station NZ04, which is located 4470 m deep at the seafloor. The infragravity peak at the deep station (NZ04) is at longer period than for the shallow station (NZ18). (c) PDFs of the temporary land station CASS. Recent recalibration of SIO OBS (see section B in the auxiliary material) suggests that OBS response values used here may be a factor of 4 too large in displacement amplitude, thus instrument corrected amplitudes may be too small. If so, this recalibration would result in the log acceleration amplitude PSD shown here increasing by a factor of $\log_{10}(16) = 1.2$.

(Figure S2a in the auxiliary material). However, when station depths do not differ a lot, the amplitude can be affected more by other factors than the depth (Figures S2a and S2b in the auxiliary material).

[10] The second microseism peak with lower amplitude and longer period (10–16 s) is known as the "single-frequency peak" (Figure 2). The origin of this peak is associated with ocean waves converted directly into seismic energy by striking the coast [*Hasselmann*, 1963]. Figure 3 shows that the amplitudes of OBS stations' single-frequency peak are smaller than those of land stations by up to 20 dB. However, *Stephen et al.* [2003] observed similar amplitudes of the single-frequency peak at OBS and island stations. We did normal mode calibration (see details in section B in the auxiliary material) for the seismic sensors to further test the instrument response parameters. The results of the normal mode calibration suggest that the nominal instrument

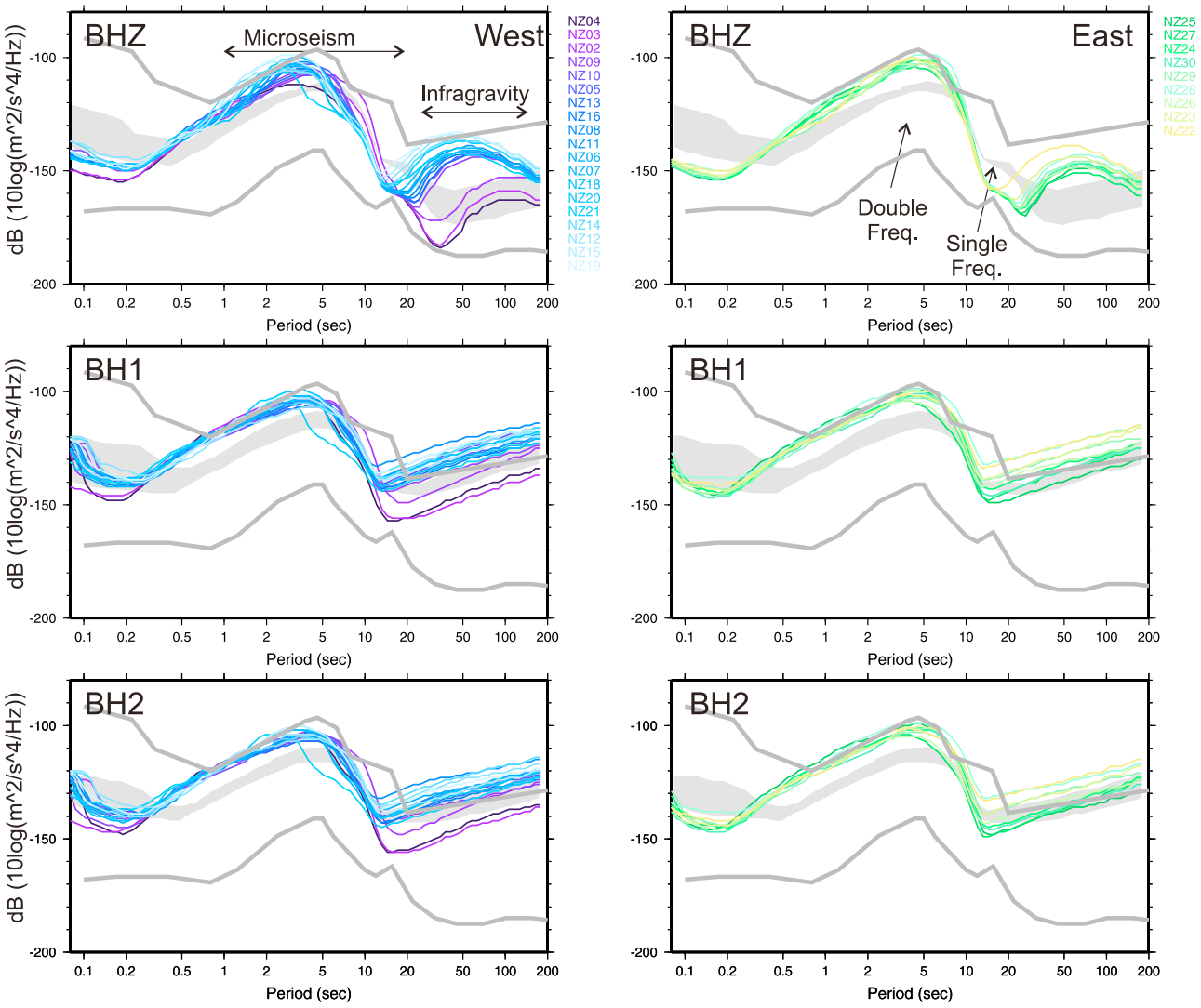

Figure 3. Median values of PDFs for all OBS stations. (left) Stations to the west of the South Island of New Zealand and (right) stations to the east of the South Island. Lines are colored according to the site depth (lighter color is shallower). A depth dependence of the peak frequency of infragravity waves is clear. Thick gray lines are the high and low noise model from *Peterson* [1993]. The gray shaded area gives the range of PDF medians for the 4 land stations on the South Island for comparison. As mentioned in Figure 3, the recalibration of SIO OBS would result in the log acceleration amplitude PSD shown here increasing by a factor of $\log_{10}(16) = 1.2$.

response may be too large by a factor of 4 but cannot rule out possible site effects. Assuming this is a frequency-independent factor, the corrected PSDs with this factor of 4 will be 16 times of the PSDs shown in Figure 3, leading to a DC up-shift of 12 dB on the log-log plots over all frequency ranges, i.e., bringing the PSDs up by 12 dB.

[11] On the other hand, *Hedlin and Orcutt* [1989] show that the noise levels of the single-frequency peak among island stations can be highly variable in both amplitude and frequency due to the interaction between the shallow continental shelf and surface gravity waves. This suggests that noise levels of the single frequency peak near New Zealand may differ from those observed in the Hawaii region [*Stephen et al.*, 2003] where the continental shelf is absent. In addition, as station depths vary from over 4 km to about 500 m, the infragravity wave peak shifts toward higher frequency at shallower depth and interferes with the single-frequency peak, affecting the noise levels of the single-frequency peak.

[12] The maximum amplitudes of microseismic peaks between OBS stations offshore the east and west coasts of New Zealand are about the same,

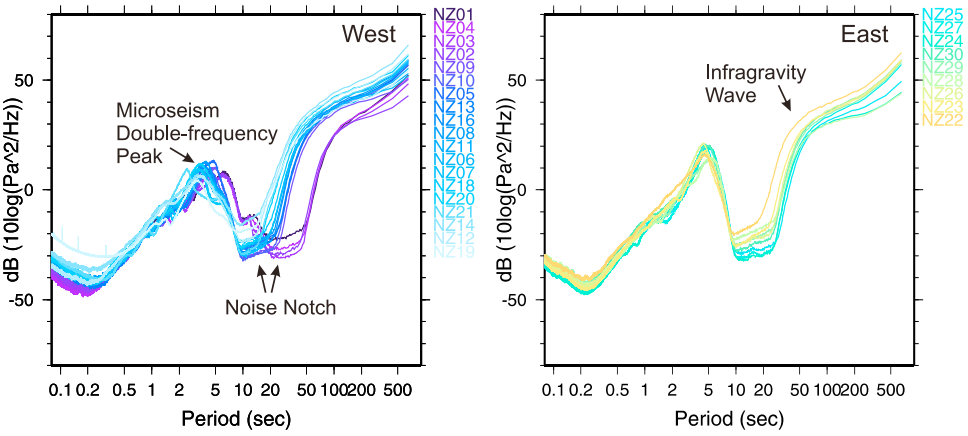

Figure 4. Year average PSDs of pressure spectrum derived from each DPG channel. (left) Stations off the west coast of New Zealand and (right) east stations. Stations are color coded according to depth (light color is shallower). Clear single-frequency microseism peak are observed for all stations. For stations at deep sea (not on continental shelf, stations NZ01, NZ02, NZ03 and NZ04), the microseisms peaks at 7 s and 14 s are clear. DPG instruments are not well calibrated and emphasis here is on the relative variation among stations as a function of depth.

around −100 dB [10log(m^2/s^4/Hz)]. However, the frequency of maximum amplitude differs between east coast and west coast OBS stations. For stations in the Tasman Sea, the maximum amplitude is at 2–5 s period, while in the Pacific Ocean the peak period is at about 5 s. The slight period shift of the microseism peak may be due to ocean climate differences. It has been noticed for a long time that peaks of microseisms evolve in concert with the local wind wave spectrum [*Webb*, 1998, and references therein] and the variability of microseism in period bands has also been noticed and studied [*Aster et al.*, 2008]. For both the eastern and western stations, near 1 s, horizontal components have higher noise levels than that the vertical component (Figure 3), which is probably due to short-wavelength shear modes and instrument coupling resonances [e.g., *Webb*, 1998; *Olofsson*, 2010].

2.2. Infragravity Wave and Noise Notch Bands

[13] Infragravity waves are water-borne surface-gravity waves at periods longer than the swell and wind-driven waves (frequencies <0.03–0.04 Hz) [e.g., *Webb et al.*, 1991]. The vertical-component PSDs show a prominent infragravity wave peak with strong depth dependence (Figure 3), as do the DPG channels (Figure 4). On the horizontal seismic components the infragravity wave peak is obscured by noise (Figure 3), though deep sites tend to have lower noise levels in general. The reason is that seafloor-currents induce ground tilt, which increases the noise levels on horizontal components as mentioned earlier.

[14] The deeper the station, the longer the period the infragravity wave peak. This is expected as the pressure signal at the seafloor of depth H is related to the surface wave height h by

$$P_{bottom} = \rho g h / \cosh(kH) \approx P_{surface} e^{kH}, \quad (1)$$

where k is the wave number ($k = 2\pi/\lambda$) and ρ is water density. If one assumes that the pressure fluctuations are caused by freely traveling surface gravity waves, the dispersion relation can be used to determine the wave number

$$\omega^2 = gk \tanh(kH), \quad (2)$$

where ω is angular frequency of the infragravity wave. If we take the product of k and H as one parameter A, equation (2) becomes

$$\omega^2 = g(A/H) \tanh(A). \quad (3)$$

[15] Now frequency f is proportional to $H^{-1/2}$, when considering A as a parameter. The peak frequency versus depth can be approximated by the relation $f_p = 0.59H^{-1/2}$, which gives $k_oH = 1.5$ at the peak frequency (Figure 5a).

[16] As the wave number $k_o = 2\pi/\lambda$, the result of a constant $k_oH = 1.5$ suggests that infragravity waves have a characteristic wavelength proportional to the inverse of the in situ depth at the seafloor, $\lambda_o = (4\pi/3)H$. This means that when water depth is known, the wavelength of the infragravity wave that generates the maximum amplitude in the seismic acceleration PSD is predictable. The constant k_oH for the seismic infragravity peak can also be used

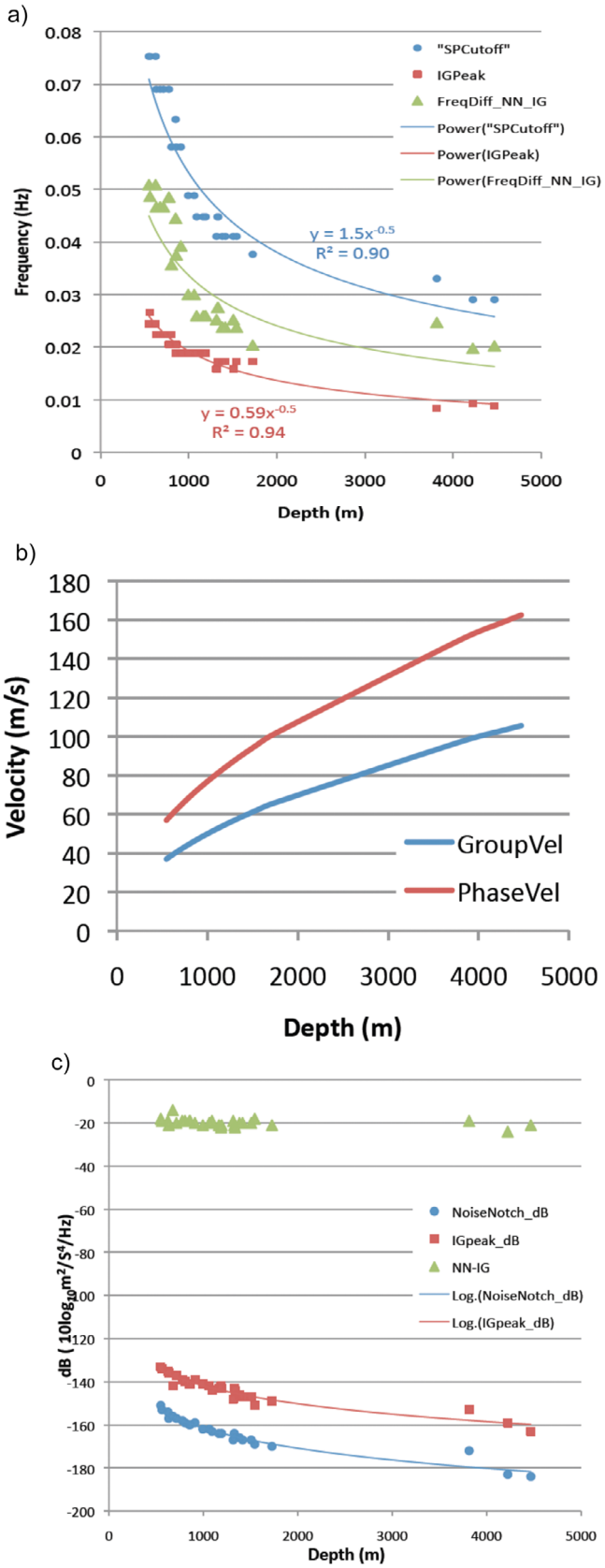
a)
"SPCutoff"
IGPeak
FreqDiff_NN_IG
Power("SPCutoff")
Power(IGPeak)
Power(FreqDiff_NN_IG)
y = 1.5x^-0.5
R² = 0.90
y = 0.59x^-0.5
R² = 0.94
Frequency (Hz)
Depth (m)
b)
Velocity (m/s)
GroupVel
PhaseVel
Depth (m)
c)
NoiseNotch_dB
IGpeak_dB
NN-IG
Log.(NoiseNotch_dB)
Log.(IGpeak_dB)
dB (10log10m²/S⁴/Hz)
Depth (m)

Figure 5

to determine the phase ($c = \omega/k$ and equation (3)) and group velocity

$$u_g = \partial\omega/\partial k = \frac{g\left(\tanh(kH) + kH/\cosh^2(kH)\right)}{\sqrt{4gk\tanh(kH)}}$$

of the infragravity wave with the characteristic wavelength λ_o at different depths. The phase velocity is a function of H, $2.43\sqrt{H}$, and for the group velocity u_g, it is $1.58\sqrt{H}$, given $k_oH = 1.5$ (Figure 5b). The k_oH value of 1.5 obtained in this study is similar to the value of k_oH of 1.4 found in French Polynesia and the Philippine Sea [*Sugioka et al.*, 2010].

[17] The plots of DPG power spectral densities in the infragravity wave band also show a depth dependent trend with period (Figure 4), although the infragravity wave peak is less well defined. The infragravity peaks in seismic acceleration PSDs (Figure 3) correspond to deflections in DPG PSDs. As station depth decreases, the deflection point goes to a shorter period (Figure 4). The deflection point is up to 60 dB [10log(Pa^2/Hz)] higher than the noise levels in the noise notch, which can be as low as −30 dB [10log(Pa^2/Hz)]. As one Pascal corresponds to a wave height of 0.1 mm, the difference of 60 dB [10log(Pa^2/Hz)] in Figure 4 can be translated into 10^4 mm^2/Hz.

[18] Infragravity waves recorded on both the seismic vertical channel and the pressure channel can be used to obtain seafloor shear modulus and hence shear velocity [e.g., *Yamamoto and Torii*, 1986; *Crawford et al.*, 1991]. The infragravity waves behave like harmonic sources for seafloor accelerations on the OBS seismometers. By measuring how much the seafloor deforms as a function of the water wavelength, the subsurface structure as a function of depth can be determined [*Crawford et al.*, 1991].

[19] When the ground acceleration reaches its peak over the infragravity wave band, that acceleration peak corresponds to the deflection point of the pressure PSDs, where the value of seafloor load (pressure) just turns to a plateau. The peak acceleration not corresponding to a maximum load is caused by the transfer function between the pressure and the seafloor vertical deformation [*Webb and Crawford*, 1999]. The relation of $k_oH = 1.5$ for the infragravity wave peak on seismic vertical acceleration PSD suggests that the infragravity wave, which excites the highest seafloor acceleration, has a characteristic wavelength proportional to the inverse of the in situ depth at the seafloor, $\lambda_o = (4\pi/3)H$.

[20] The frequency band bounded by the infragravity waves at 0.03 Hz and the microseisms at 0.1 Hz, is the so-called "noise notch" [e.g., *Webb*, 1998]. The short-period cutoff of infragravity waves is the long-period cutoff of the noise notch. Figure 5 shows the depth dependence of the periods of short-period cutoff. Using equation (3), the relationship between the site depth and the periods of the short-period cutoff can be expressed as $f_s = 1.5H^{-1/2}$, which gives the value of the product of the wave number and water depth kH as 9.1. The value of kH for the short-period cutoff of infragravity waves is 10.1 in Monterey Bay [*Dolenc et al.*, 2005]. The noise notch is important for long period seismic body and surface wave studies because there are no major noise sources in this band thus yielding a larger signal-to-noise ratio for seismic waves in this band. Stations NZ02 and NZ03, which are deeper than 4000 m, have noise notches between 20 s and 50 s with power levels as low as −184 and −183 dB [10log(m^2/s^4/Hz)], respectively (Figure 3). For stations at shallower depths, the noise notches shift to shorter periods as short as 13.3 s for the depth of about 550 m (NZ19) and 560 m (NZ15). The power levels between 20 s and 50 s range from −165 to about −130 dB [10log(m^2/s^4/Hz)], when the site depth increases from about 550 m to over 1700 m. This is a difference of 18 to 53 dB [10log(m^2/s^4/Hz)] comparing with stations deeper than 4000 m.

[21] Although the period of the peak and short-period cutoff of infragravity waves decreases with site depth (Figure 5a), the difference of noise power between the peak and the short-period cutoff on vertical acceleration PSDs stays constant at about −20 dB [10log(m^2/s^4/Hz)] (Figure 5c). The experimental depth dependence of the maximum amplitude

Figure 5. (a) Observed frequency of infragravity wave peak (red squares) and noise notch (blue circles) versus depth for vertical seismic component OBS. The data is well fit with the relation $f_p = 0.59H^{-1/2}$ for the peak frequency (red) and $f_s = 1.5H^{-1/2}$ for the short-period cutoff (blue), giving values of kH of 1.5 and 9.1, respectively. R^2 refers to the square of the correlation coefficient between the data points and the fitting line. When R is ±1, the fitting is perfect. The bandwidth between the peak and the short-period cutoff at each depth is shown in green triangles. (b) Estimated phase (red) and group (blue) velocity of infragravity wave as a function of water depth, given $k_oH = 1.5$. (c) Observed maximum spectral amplitudes of the infragravity wave at peak frequency (red squares) and minimum spectral amplitude of the noise notch (blue circles) versus depth for each OBS site. The difference between the two values for each depth is in green triangles.

of infragravity peak and the minimum amplitude of noise notch in the PSDs are obtained from our analysis (Figure 5c). The experimental depth dependence can be used to estimate the expected amplitudes of infragravity peak and noise notch in the PSDs, which is useful for the design of OBS experiments.

3. Conclusions

[22] In addition to quantifying ambient noise offshore New Zealand, we obtain two general results regarding the characteristics of infragravity waves. First, our results present a clear depth dependence of infragravity wave peak frequency (Figure 5), described by the relationship $k_oH = 1.5$. Thus infragravity waves have a characteristic wavelength at their peak frequency, and this relationship can be used to determine phase and group velocity of the infragravity wave. Second, the equations that we have determined to describe the depth dependence of the maximum noise level of the infragravity peak and the minimum noise level of noise notch can be used to estimate noise levels at any depth. These relations can be used in OBS experiment design and planning. Future work will explore whether these relations derived from offshore New Zealand apply to other oceans.

Acknowledgments

[23] The instruments used in this field program were provided by the U.S. National Ocean Bottom Seismic Instrumentation Pool (http://www.obsip.org). Seismic data are archived at the IRIS Data Management Center. The figures were made using Generic Mapping Tools (GMT) software by *Wessel and Smith* [1998]. We thank captain and crew of the R/V Thomas G. Thompson (cruise TN229) in 2009, of the R/V Roger Revelle (cruise RR1002) in 2010, and SIO OBSIP field engineers for expert assistance with deployment and recovery of the OBS instruments. We thank Peter Molnar, Oleg Godin, Nikolay Zabotin, and Justin Ball for helpful discussions. Z.Y. gratefully acknowledges the IRIS/PASSCAL Graduate Student Internship that provided her the opportunity and the training to study seismic noise. The collection of OBS data was supported by the National Science Foundation Continental Dynamics program under grants EAR-0409564, EAR-0409609, and EAR-0409835. The authors thank G-cubed editor Thorsten Becker, associate editor Robert Dunn, and two anonymous reviewers for constructive comments which led to significant improvements in the manuscript.

References

Aster, R., D. McNamara, and P. Bromirski (2008), Multidecadal climate-induced variability in microseisms, *Seismol. Res. Lett.*, *79*, 194–202, doi:10.1785/gssrl.79.2.194.

Bradley, C. R., R. A. Stephen, R. A. Dorman, and J. A. Orcutt (1997), Very low frequency (0.2–10.0 Hz) seismoacoustic noise below the seafloor, *J. Geophys. Res.*, *102*, 11,703–11,718, doi:10.1029/96JB03183.

Bromirski, P. D., F. K. Duennebier, and R. A. Stephen (2005), Mid-ocean microseisms, *Geochem. Geophys. Geosyst.*, *6*, Q04009, doi:10.1029/2004GC000768.

Collins, J. A., F. L. Vernon, J. A. Orcutt, R. A. Stephen, K. R. Peal, F. B. Wooding, F. N. Spiess, and J. A. Hildebrand (2001), Broadband seismology in the oceans: Lessons from the Ocean Seismic Network Pilot Experiment, *Geophys. Res. Lett.*, *28*(1), 49–52.

Cox, C., T. Deaton, and S. Webb (1984), A deep-sea differential pressure gauge, *J. Atmos. Oceanic Technol.*, *1*, 237–246, doi:10.1175/1520-0426(1984)001<0237:ADSDPG>2.0.CO;2.

Crawford, W., S. C. Webb, and J. A. Hidebrand (1991), Seafloor compliance observed by long-period pressure and displacement measurements, *J. Geophys. Res.*, *96*, 16,151–16,160, doi:10.1029/91JB01577.

Dolenc, D., B. Romanowicz, D. Stakes, P. McGill, and D. Neuhauser (2005), Observations of infragravity waves at the Monterey ocean bottom broadband station (MOBB), *Geochem. Geophys. Geosyst.*, *6*, Q09002, doi:10.1029/2005GC000988.

Dolenc, D., B. Romanowicz, P. McGill, and W. Wilcock (2008), Observations of infragravity waves at the ocean-bottom broadband seismic stations Endeavour (KEBB) and Explorer (KXBB), *Geochem. Geophys. Geosyst.*, *9*, Q05007, doi:10.1029/2008GC001942.

Duennebier, F. K., and G. Sutton (2007), Why bury ocean bottom seismometers?, *Geochem. Geophys. Geosyst.*, *8*, Q02010, doi:10.1029/2006GC001428.

Hasselmann, K. (1963), A statistical analysis of the generation of microseisms, *Rev. Geophys.*, *1*(2), 177–210, doi:10.1029/RG001i002p00177.

Hedlin, M. A. H., and J. A. Orcutt (1989), A comparative study of island, seafloor, and subseafloor ambient noise levels, *Bull. Seismol. Soc. Am.*, *79*(1), 172–179.

Longuet-Higgins, M. S. (1950), A theory of the origin of microseisms, *Philos. Trans. R. Soc.*, *243*, 1–35, doi:10.1098/rsta.1950.0012.

McCreery, C. S. (1992), Long-term ambient ocean noise, 0.05–30 Hz from the Wake Island Hydrophone Array, PhD thesis, 119 pp., Univ. of Hawai'i at Mānoa, Honolulu.

McNamara, D., and R. Boaz (2006), Seismic noise analysis system using power spectral density probability density functions—A stand-alone software package, *U.S. Geol. Surv. Open File Rep.*, *2005-1438*, 29 pp.

McNamara, D., and R. P. Buland (2004), Ambient noise levels in the continental United States, *Bull. Seismol. Soc. Am.*, *94*, 1517–1527, doi:10.1785/012003001.

Olofsson, B. (2010), Marine ambient seismic noise in the frequency range 1–10 Hz, *Leading Edge*, *29*(4), 418–435 doi:10.1190/1.3378306.

Peterson, J. (1993), Observation and modeling of seismic background noise, *U.S. Geol. Surv. Open File Rep.*, *93-322*, pp. 1–95.

Sorrells, G. G. (1971), A preliminary investigation into the relationship between long-period seismic noise and local fluctuations in the atmospheric pressure field, *Geophys. J. R. Astron. Soc.*, *26*, 71–82, doi:10.1111/j.1365-246X.1971.tb03383.x.

Stephen, R. A., F. N. Spiess, J. A. Collins, J. A. Hildebrand, J. A. Orcutt, K. R. Peal, F. L. Vernon, and F. B. Wooding

(2003), Ocean Seismic Network Pilot Experiment, *Geochem. Geophys. Geosyst.*, *4*(10), 1092, doi:10.1029/2002GC000485.

Sugioka, H., Y. Fukao, and T. Kanazawa (2010), Evidence for infragravity wave-tide resonance in deep oceans, *Nat. Commun.*, *1*, 84, doi:10.1038/ncomms1083.

Webb, S. (1988), Long-period acoustic and seismic measurements and ocean floor currents, *J. Oceanic Eng.*, *13*(4), 263–270, doi:10.1109/48.9239.

Webb, S. (1998), Broadband seismology and noise under the ocean, *Rev. Geophys.*, *36*(1), 105–142, doi:10.1029/97RG02287.

Webb, S., and W. Crawford (1999), Long-period seafloor seismology and deformation under ocean waves, *Bull. Seismol. Soc. Am.*, *89*(6), 1533–1542.

Webb, S., X. Zhang, and W. Crawford (1991), Infragravity waves in the deep ocean, *J. Geophys. Res.*, *96*(C2), 2723–2736, doi:10.1029/90JC02212.

Wessel, P., and W. H. F. Smith (1998), New, improved version of Generic Mapping Tools released, *Eos Trans. AGU*, *79*(47), 579, doi:10.1029/98EO00426.

Wilson, D., D. Leon, R. Aster, J. Ni, J. Schlue, S. Grand, S. Semken, and S. Baldridge (2002), Broadband seismic background noise at temporary seismic stations observed on a regional scale in the southwestern United States, *Bull. Seismol. Soc. Am.*, *92*, 3335–3342, doi:10.1785/0120010234.

Withers, M., R. Aster, C. Young, and E. Chael (1996), High-frequency analysis of seismic background noise and signal-to-noise ratio near Datil, New Mexico, *Bull. Seismol. Soc. Am.*, *86*, 1507–1515.

Yamamoto, T., and T. Torii (1986), Seabed shear modulus profile inversion using surface gravity wave induced bottom motion, *Geophys. J. R. Astron. Soc.*, *85*, 413–431, doi:10.1111/j.1365-246X.1986.tb04521.x.